

# Laser-induced reduction and in-situ optical spectroscopy of individual plasmonic copper nanoparticles for catalytic reactions

G. Di Martino, V. A. Turek, P. Braeuninger-Weimer, S. Hofmann, and J. J. Baumberg

Citation: *Appl. Phys. Lett.* **110**, 071111 (2017); doi: 10.1063/1.4976694

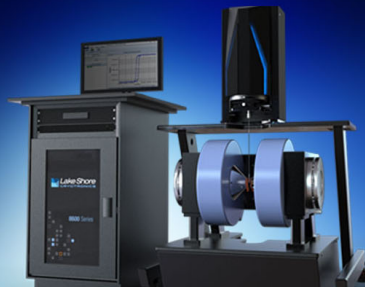
View online: <http://dx.doi.org/10.1063/1.4976694>

View Table of Contents: <http://aip.scitation.org/toc/apl/110/7>

Published by the [American Institute of Physics](#)

---

---



## NEW 8600 Series VSM

For fast, highly sensitive  
measurement performance

LEARN MORE 

# Laser-induced reduction and in-situ optical spectroscopy of individual plasmonic copper nanoparticles for catalytic reactions

G. Di Martino,<sup>1,a)</sup> V. A. Turek,<sup>1</sup> P. Braeuninger-Weimer,<sup>2</sup> S. Hofmann,<sup>2</sup> and J. J. Baumberg<sup>1</sup>

<sup>1</sup>NanoPhotonics Centre, Cavendish Laboratory, University of Cambridge, CB3 0HE Cambridge, United Kingdom

<sup>2</sup>Department of Engineering, University of Cambridge, CB3 0FA Cambridge, United Kingdom

(Received 17 October 2016; accepted 2 February 2017; published online 16 February 2017)

Copper (Cu) can provide an alternative to gold (Au) for the development of efficient, low-cost and low-loss plasmonic nanoparticles (NPs), as well as selective nanocatalysts. Unlike Au, the surface oxidation of Cu NPs can be an issue restricting their applicability. Here, we selectively reduce the Cu NPs by low power laser illumination in vacuum and use dark-field scattering to reveal in real time the optical signatures of the reduction process and its influence on the Cu NP plasmonic resonance. We then study reactive processes at the single particle level, using individual Cu catalyst nanoparticles for the selective laser-induced chemical vapour deposition of germanium nanostructures. © 2017 Author(s). All article content, except where otherwise noted, is licensed under a Creative Commons Attribution (CC BY) license (<http://creativecommons.org/licenses/by/4.0/>). [<http://dx.doi.org/10.1063/1.4976694>]

Metal nanoparticles (NPs) have been extensively studied in recent years due to their wide range of potential applications in the fields of catalysis,<sup>1,2</sup> light harvesting,<sup>3,4</sup> sensing,<sup>5</sup> and surface-enhanced Raman scattering.<sup>6</sup> Moreover, the high field confinement due to localised plasmonic resonances is used in several processes.<sup>7,8</sup> The most commonly used plasmonic metals are gold (Au) and silver (Ag), but alternative materials have lately been explored.<sup>9</sup> Among them, a low-cost alternative is copper (Cu), which has the second-best conductivity among metals (next to silver), shows catalytic behaviours for CMOS-compatible nanowire (NW) synthesis,<sup>10,11</sup> and is already widely used as interconnect material in integrated circuits.

However, the focus of the scientific community on gold and silver has resulted in the absence of a well-established procedure for the synthesis of Cu NPs with the subsequent lack of homogeneity in the size and shape of the synthesized Cu NPs.<sup>12–14</sup> In addition, fabricating devices with copper NPs is challenging, as they easily oxidize to form Cu<sub>2</sub>O and CuO. Moreover, the back-end device integration requires process temperatures <450 °C, which is a challenge for standard Cu catalysed nanowire synthesis.

In this work, we address these issues by synthesizing and investigating different-sized Cu NPs. We use laser irradiation and selective absorption to locally heat and reduce one NP at a time in a vacuum chamber upon illumination with a 532 nm laser beam. Through in-situ dark-field spectroscopy, the NP reduction process is observed from its changing optical signature in real time, showing a blue shift of the plasmonic resonance in the scattering spectra. We then use the reduced Cu NPs for the light-induced catalytic growth of Ge nanocrystals, in a process that resembles the previously reported growth of Au catalysed nanowires (NWs).<sup>2</sup> Here, the reaction is not triggered by global heating of the sample to high temperatures (which limits the choice

of substrate and device integration pathways) but by local heating of the catalyst seed without any effect on the surrounding substrate, which results in a technique compatible with back-end device integration and CMOS processing.

The Cu NPs were synthesised using reagents bought from Sigma-Aldrich and used without further purification. The synthesis involves dissolution of 62.4 mg CuSO<sub>4</sub>·5H<sub>2</sub>O (99.995%) and 200 mg polyvinylpyrrolidone (PVP, m.w. 40,000) in 45 ml diethylene glycol (≥99.0%), and to this, 44 mg sodium hypophosphite (≥99.0%) in 15 ml diethylene glycol is added heating up to 200 °C. Then, 25 mg ascorbic acid (≥99.0%) is added prompting the solution to change colour from the initial light-blue to green, then to black and finally to a dark brown. In order to select particles in the ~100 nm diameter range, the 1 ml of solution is centrifuged at 1000 RPM for 5 minutes and the supernatant extracted and centrifuged for 2000 RPM for 5 min. The supernatant of the 2<sup>nd</sup> centrifugation is discarded, and the sedimented particles are diluted in 1 ml methanol followed by 3 further centrifugation–methanol dilution cycles at 2000 RPM for 5 min and a final concentration step without dilution. The resulting volume of the sample is ~50 μl. The extracted particles are then deposited onto a 20 nm thin silicon nitride substrate by drying a 10 μl aliquot of the sample onto the substrate, which is subsequently washed 3 times with methanol.

We previously reported the selective laser-induced chemical vapour deposition (CDV) of single Au seeded germanium nanowires, where the dark-field scattering of this system reveals in real time the optical signatures of all key constituent growth processes.<sup>2</sup> Here, we aim to investigate the laser-induced chemical vapour deposition with catalysts such as Cu NPs. As previously discussed, Cu oxidizes to form Cu<sub>2</sub>O and CuO, and therefore laser irradiation and selective light absorption is first used to locally heat and trigger the reduction of individual Cu NPs (Fig. 1). We use a customised stainless-steel vacuum chamber (base pressure ~10<sup>-7</sup> mbar), in which we selectively illuminate well-separated (average distance

<sup>a)</sup>E-mail: gd392@cam.ac.uk

$>5 \mu\text{m}$ ) Cu NPs on a 20 nm-thin transparent silicon nitride membrane with a continuous wave laser at  $\lambda = 532 \text{ nm}$ . Dark field spectra are collected by scattering unpolarised white light focussed from the back of the transparent membrane supporting the Cu NPs.

The plasmonic optical signature of interest is known as the localised surface plasmon resonance (LSPR). The LSPR is excited when light interacts with the free (conduction) electrons of a metallic nanostructure, which results in collective excitations (oscillations) that lead to a strong enhancement of the local electromagnetic field surrounding the nanoparticles.<sup>15</sup> We exploit the heat generated by metal NPs under optical illumination to serve as highly efficient localized heat sources on the nanometer-length scale.<sup>16–19</sup> Enhanced light absorption due to the presence of a plasmonic resonance is followed by carrier relaxation, which heats the metallic nanostructures. Fast thermal diffusion leads to uniform NP temperatures.<sup>20</sup> The heat is then transferred to the surroundings of the metal within 100 ps–10 ns, depending on the material, particle size and surrounding thermal conductivity as well as the thermal contact to the substrate.<sup>17,21,22</sup> The thermal conductivity for the materials studied is high, and the length scales of the structures are small. NPs reach thermal equilibrium in a time<sup>23</sup>  $\tau = R^2 C_p^2 / 9 C_s \Lambda_s$ , where  $C_s$  is the heat capacity (per unit volume) of the shell,  $C_p$  is the heat capacity of the Cu, and  $\Lambda_s$  is the thermal conductivity of the shell. For the particles here, we estimate that the system reaches a thermal equilibrium in  $\sim 1 \text{ ns}$ . Therefore, it is safe to assume that the catalyst nanoparticle and the surrounding oxide have the same temperature given the vacuum atmosphere. It is thus this optical-triggered heating of the outer oxide shell that induces the reduction process. The presence of the oxide shell and its reduction have a strong effect on the plasmonic modes of Cu NPs.<sup>24</sup> Their frequency

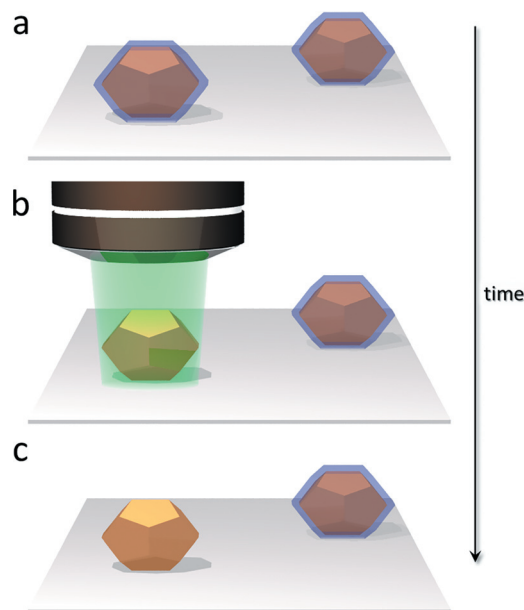


FIG. 1. Cu NP reduction. Schematic of selective reduction of Cu NPs by laser illumination. The 532 nm laser is focused to  $1 \mu\text{m}$  spot size. (a) Initially, the Cu NPs have not been illuminated and an outer oxide layer, depicted in blue, is present. (b) In the next step, one Cu NP is illuminated by the laser beam, so that (c) the outer layer of copper oxide is reduced after laser illumination.

and spectral widths are determined by the electron density, effective mass, particle shape and size, dielectric function, and surrounding environment. Electron density, effective mass and dielectric function are characteristics of the material, which were therefore fixed in our experiment. From SEM characterization, the nanoparticles we illuminate show the same spherical shape before and after irradiation (Fig. 2 inset, Fig. 3(a), Fig. S2 of supplementary material). Therefore, any change we observe in the scattering signal must originate the modification of the two remaining parameters: the NP size and its surrounding environment. The scattering spectra recorded for different sized Cu NPs (Figs. 2(a)–2(c)) show that exposure to the laser beam blue-shifts the LSPR. The change in size alone is unable to account for the large spectral shifts ( $>100 \text{ nm}$ ) we report. Therefore, the change in the environment of the metal NP, i.e., the oxide thickness, unequivocally explains the experimental observations. In order to be able to better resolve the spectral dynamics, we use a low laser power (1.5 mW) such that the whole reduction process takes  $\sim 100 \text{ s}$ . This behaviour is exhibited for all the different sized NPs studied here ( $\sim 100\text{--}300 \text{ nm}$ ), demonstrating that the effects of the oxide shell are relatively

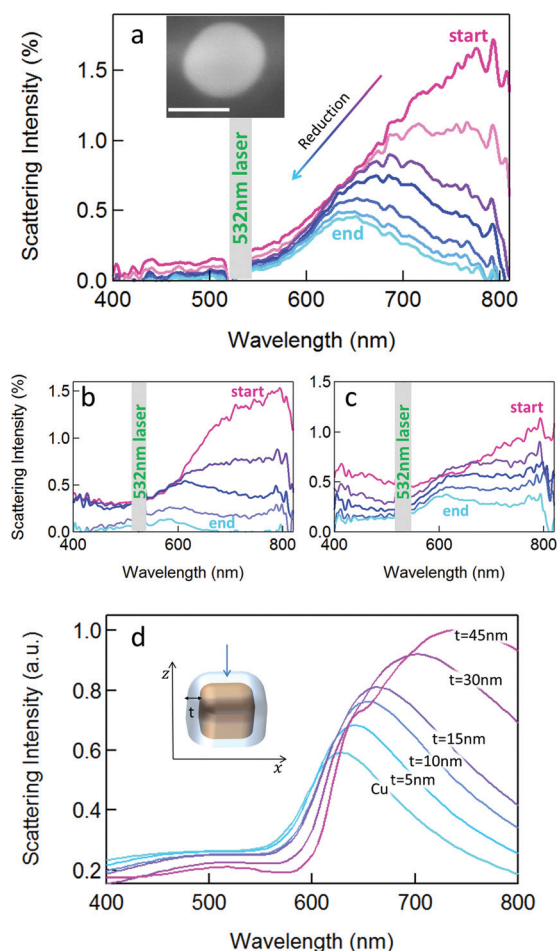


FIG. 2. Cu NPs' reduction. Scattering spectra of individual Cu NPs irradiated by 532 nm laser beam in vacuum for NP diameters of (a) 130 nm, (b) 100 nm, and (c) 150 nm. Inset, SEM image of Cu NP after irradiation. Scale bar is 100 nm. (d) Simulated scattering spectra of rounded Cu cube of side length 140 nm with progressively reducing thickness  $t$  of oxide shell. In all simulations, incident Gaussian light (blue arrow) is polarised along  $x$  and propagating along  $-z$  direction.

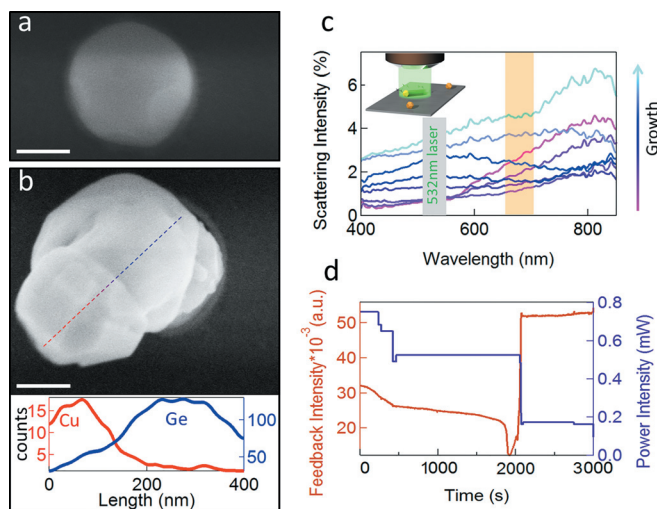


FIG. 3. Cu-catalysed Ge growth. Reduced Cu NP before (a) and after (b) growth process. Cu NP diameter  $\sim 220$  nm. Inset, energy-dispersive X-ray (EDX) spectroscopy along the dashed line shows the presence of Cu in red and Ge in blue in the grown structure. Scale bar is 100 nm. (c) Evolution of scattering spectra during growth with (d) corresponding feedback control that reduces the laser power (purple line) when a change in the scattering signal (orange line, integrated over spectral range 650–700 nm; orange shaded area in (c)) is detected. Dynamically reducing the irradiation laser power avoids overheating, enabling the controllable growth of Ge NWs.

independent of the particle size (phase retardation effects for the larger particles play only a minor role in the observed LSPR variations). The thinning of the oxide layer also reduces the intensity of the LSPR. This is because the blueshift brings the LSPR peak inside the spectral region of copper interband transitions, more strongly damping the plasmon due to its interaction with the absorption background, resulting in a decrease in intensity. We confirm these observations by simulating the optical response of core-shell (Cu@Cu<sub>2</sub>O) structures with geometries, as shown in the inset of Fig. 2(d), for different oxide thicknesses  $t$ . We use standard finite-difference time-dependent simulations (Lumerical),<sup>25</sup> illuminating a Cu cube of side 140 nm with rounded corners to model the NPs. Indeed, a blueshift and an intensity reduction of the LSPR peak are observed for thinner oxide layers (Fig. 2(d)) matching our experimental data.

Native copper oxide is a mixture of CuO and Cu<sub>2</sub>O (Pilling-Bedworth ratio 1.78 and 1.12, respectively).<sup>26</sup> In-situ SEM analysis during the in-vacuum heating of Cu NPs (up to  $\sim 830$  °C) confirms that a decrease in volume occurs during the NP reduction of the copper. We observe a volume decrease by a factor of 6 of the reduced particles after annealing, compared to their initial volume with native oxide layer (supplementary material, Fig. (S1)). For comparison, the volume ratio extrapolated from the simulations of the rounded Cu cube with a 45 nm oxide shell is 4.4. We thereby infer that the range of temperatures achieved during laser heating is comparable to those during the in-situ heating in the SEM. The Cu NP shapes observed in electron microscopy after irradiation (Fig. 2(a), inset) appear much more homogeneous compared to the initial non-irradiated nanostructures (supplementary material Fig. (2)). They also appear generally similar to each other, and thus our technique of irradiation offers an alternative solution to the challenge of

generating homogenous Cu seed NPs, without the need to expose the whole substrate to high temperatures.

The photo-switchable oxidation states of functioning catalysts result in a valuable tool for the control of surface reactions.<sup>27</sup> The reduction of Cu<sub>x</sub>O to bare Cu NPs at the single particle level and the possibility to observe the spectroscopic signature of any process in vacuum conditions or in the presence of a gaseous species opens up the possibility to study systems and explore chemical reactions through optical spectroscopy in real time. We aim to study the reactive processes at the single particle level and here focus on the laser-induced catalytic growth of germanium nanostructures from the reduced Cu NPs (Fig. 3(a)). We introduce diluted Ge<sub>2</sub>H<sub>6</sub> as the precursor (0.2% in Ar,  $\sim 10$  mbar total pressure during growth) into the vacuum chamber. Depending on the catalyst particle temperature, material growth is achieved either with the catalyst remaining in a solid phase (including germanide phase transformations) or as the catalyst forms a liquid alloy phase (which generally leads to faster growth rates<sup>2,28,29</sup>).

We use laser irradiation and selective light absorption to locally heat and trigger reactions on individual supported catalyst nanoparticles in the gaseous precursor atmosphere, using a technique developed previously.<sup>2</sup> In line with the previous detailed growth studies,<sup>11,29</sup> this leads to a local and selective Ge<sub>2</sub>H<sub>6</sub> dissociation on the Cu NP. The reaction/dissolution and eventual supersaturation with Ge triggers the nucleation and growth of a Ge crystal. For excessively high temperatures (i.e., at too high laser power), non-selective pyrolytic decomposition of the Ge precursor dominates. Hence, the restriction of laser powers is important to ensure a selective growth process that occurs only on the catalyst interface and in particular, not on the adjacent substrate that is also heated. In fact, as we previously highlighted,<sup>2</sup> such laser control of catalytic crystal growth is non-trivial as the phase transformations of the catalyst as well as the growing crystal cause a continuous reaction-dependent change in laser absorption. As the Ge crystal grows, the composite nanostructure absorbs more and more light because of the increasing optical cross-section, observed simultaneously as a rise in scattering strength (Fig. 3(c)). The complex spectral signal we detect is induced by the presence of localised magnetic and electric resonances supported in the Ge nanostructure, which dominate the optical response.<sup>2</sup> Such resonances can be spectrally tuned by varying the crystal length and diameter.<sup>30</sup> As we previously reported,<sup>2</sup> the spectral positions of the resonances for different modes excited inside an NW show a general redshift with increasing NW length. This enables us to follow the crystal elongation during growth. In the spectra of Fig. 3(c), the transverse-magnetic TM<sub>11</sub> resonance redshifts into the infrared wavelength range, outside the detected region. As the crystal length increases further, the transverse-electric TE<sub>11</sub> resonance, which initially lies in the visible region, redshifts to  $\sim 800$  nm and increases its intensity. Such optical signatures allow us to follow in real time the growth of the Ge crystal, which is however not the main focus of the current paper. It is important to note that if the laser power is not reduced accordingly to keep the temperature constant, this leads to positive feedback and detrimental overheating with the temperatures then high enough to cause non-selective, deleterious pyrolytic Ge

overgrowth.<sup>2</sup> In order to avoid such overheating, we thus use the scattered intensity as a control signal to directly adjust the power of the laser during the reaction (see Fig. 3(d)). By implementing this in-situ feedback, we maintain the catalytic process to be dominant and can show the early stages of localised crystal growth (Fig. 3(b)). We do not observe any growth if we irradiate the substrate without nanoparticles. We note that the laser spot has a diameter of 2  $\mu\text{m}$  and the largest particle we irradiate is  $\sim 200\text{nm}$ . We observe growth only from the copper and not on the surrounding substrate. Thus, we emphasise that only the Cu nanoparticles are active here, and they act as seeds for nucleation.

In this work, we show in-situ observations of the reduction of copper oxide around Cu NPs upon laser irradiation. By combining low pressure and high temperature conditions, it becomes possible to reverse the native oxidation process, leading to the recovery of pure copper particles. We examine in real time the optical response of the system by dark field spectroscopy observing blue-shifts and a reduction in intensity of the Cu NP plasmonic resonance on reduction. This technique operates at very low mW laser powers due to slow heat dissipation within the thin support membrane. This capability to easily reduce copper oxide NPs by light indicates that Cu may now be able to replace the more expensive metals of Ag and Au for certain plasmonic applications, including refractive-index sensing and surface enhanced Raman spectroscopy (SERS) in gas-phase applications.<sup>31</sup> We also demonstrate one particular application of Cu NPs, using them to selectively drive catalytic growth reactions at low laser power ( $<1\text{ mW}$ ). Our results show the capability to grow the CMOS-compatible metal-catalysed nanostructures by locally heating the CuNP catalyst via laser irradiation, while optically monitoring their spectroscopic signature, leaving nearby regions unreacted. Our technique can also be applied to study a range of crystal growth reactions on the nano-scale, allowing rapid facile combinatorial mapping and screening of the CVD parameter space, which is arduous with conventional global back heating.

See [supplementary material](#) for Cu NPs' volume change with heating, SEM characterization of initially synthesised Cu NPs and absorption in Cu oxides.

We acknowledge the financial support from EPSRC Grant Nos. EP/G060649/1, EP/L027151/1, and EP/G037221/1, and ERC Grant No. LINASS 320503. S.H. acknowledges the funding from the ERC grant InsituNANO 279342. We acknowledge Eugen Hildebrandt for helping with the insitu ESEM annealing. Source data can be found at <https://doi.org/10.17863/CAM.7582>.

- <sup>1</sup>J. M. Kum, Y. J. Park, H. J. Kim, and S. O. Cho, *Nanotechnology* **26**, 125402 (2015).
- <sup>2</sup>G. Di Martino, F. B. Michaelis, A. R. Salmon, S. Hofmann, and J. J. Baumberg, *Nano Lett.* **15**, 7452 (2015).
- <sup>3</sup>H. A. Atwater and A. Polman, *Nat. Mater.* **9**, 205 (2010).
- <sup>4</sup>J. Trevino, C. Forestiere, G. Di Martino, S. Yerci, F. Priolo, and L. Dal Negro, *Opt. Express* **20**, A418 (2012).
- <sup>5</sup>J. N. Anker, W. P. Hall, O. Lyandres, N. C. Shah, J. Zhao, and R. P. Van Duyne, *Nat. Mater.* **7**, 442 (2008).
- <sup>6</sup>V. V. Thacker, L. O. Herrmann, D. O. Sigle, T. Zhang, T. Liedl, J. J. Baumberg, and U. F. Keyser, *Nat. Commun.* **5**, 3448 (2014).
- <sup>7</sup>R. W. Taylor, F. Benz, D. O. Sigle, R. W. Bowman, P. Bao, J. S. Roth, G. R. Heath, S. D. Evans, and J. J. Baumberg, *Sci. Rep.* **4**, 5940 (2014).
- <sup>8</sup>G. Di Martino, S. Tappertzhofen, S. Hofmann, and J. Baumberg, *Small* **12**, 1334 (2016).
- <sup>9</sup>P. R. West, S. Ishii, G. V. Naik, N. K. Emani, V. M. Shalae, and A. Boltasseva, *Laser Photonics Rev.* **4**, 795 (2010).
- <sup>10</sup>V. T. Renard, M. Jublot, P. Gergaud, P. Cherns, D. Rouchon, A. Chabli, and V. Jousseume, *Nat. Nanotechnol.* **4**, 654 (2009).
- <sup>11</sup>C.-Y. Wen, M. C. Reuter, J. Tersoff, E. A. Stach, and F. M. Ross, *Nano Lett.* **10**, 514 (2010).
- <sup>12</sup>D. Mott, J. Galkowski, L. Wang, J. Luo, and C.-J. Zhong, *Langmuir* **23**, 5740 (2007).
- <sup>13</sup>M. S. Usman, M. E. E. Zowalaty, K. Shameli, N. Zainuddin, M. Salama, and N. A. Ibrahim, *Int. J. Nanomed.* **8**, 4467 (2013).
- <sup>14</sup>K. S. Tan and K. Y. Cheong, *J. Nanopart. Res.* **15**, 1537 (2013).
- <sup>15</sup>*Absorption and Scattering of Light by Small Particles*, edited by C. F. Bohren and D. R. Huffman (Wiley-VCH Verlag GmbH, Weinheim, Germany, 1998).
- <sup>16</sup>G. Baffou and R. Quidant, *Laser Photonics Rev.* **7**, 171 (2013).
- <sup>17</sup>M. L. Brongersma, N. J. Halas, and P. Nordlander, *Nat. Nanotechnol.* **10**, 25 (2015).
- <sup>18</sup>Z. Fang, Y.-R. Zhen, O. Neumann, A. Polman, F. J. García de Abajo, P. Nordlander, and N. J. Halas, *Nano Lett.* **13**, 1736 (2013).
- <sup>19</sup>O. A. Yeshchenko, N. V. Kutsevov, and A. P. Naumenko, *Plasmonics* **11**, 345 (2016).
- <sup>20</sup>G. Baffou, R. Quidant, and C. Girard, *Appl. Phys. Lett.* **94**, 153109 (2009).
- <sup>21</sup>H. H. Richardson, M. T. Carlson, P. J. Tandler, P. Hernandez, and A. O. Govorov, *Nano Lett.* **9**, 1139 (2009).
- <sup>22</sup>G. Baffou, R. Quidant, and F. J. García de Abajo, *ACS Nano* **4**, 709 (2010).
- <sup>23</sup>O. M. Wilson, X. Hu, D. G. Cahill, and P. V. Braun, *Phys. Rev. B* **66**, 224301 (2002).
- <sup>24</sup>G. H. Chan, J. Zhao, E. M. Hicks, G. C. Schatz, and R. P. Van Duyne, *Nano Lett.* **7**, 1947 (2007).
- <sup>25</sup>A commercial simulator based on finite-difference time-domain method was used to perform the calculations of the far-field extinction spectra and near-field distributions (Lumerical Solutions Inc.). Perfectly matched layer (PML) absorbing boundaries conditions have been implemented. A 0.5 nm mesh has been used. The simulated source is a broadband Gaussian beam polarised along (see Figure 2) and propagating along  $-z$ .
- <sup>26</sup>P. Keil, D. Lützenkirchen-Hecht, and R. Frahm, *AIP Conf. Proc.* **882**, 490 (2007).
- <sup>27</sup>A. Marimuthu, J. Zhang, and S. Linic, *Science* **339**, 1590 (2013).
- <sup>28</sup>R. S. Wagner and W. C. Ellis, *Appl. Phys. Lett.* **4**, 89 (1964).
- <sup>29</sup>S. Hofmann, R. Sharma, C. T. Wirth, F. Cervantes-Sodi, C. Ducati, T. Kasama, R. E. Dunin-Borkowski, J. Drucker, P. Bennett, and J. Robertson, *Nat. Mater.* **7**, 372 (2008).
- <sup>30</sup>J. van de Groep and A. Polman, *Opt. Express* **21**, 26285 (2013).
- <sup>31</sup>G. C. Schatz and R. P. Van Duyne, *Handbook of Vibrational Spectroscopy* (John Wiley & Sons, Ltd., 2006).